Reprinted from INTERNATIONAL JOURNAL OF THERMOPHYSICS

Vol. 8, No. 2, March 1987
Printed in Belgium

Thermal Diffusivity of Fluids in a Broad Region Around the Critical Point

P. Jany[1] **and J. Straub**[1]

Received March 24, 1986

Dynamic light scattering is a suitable method for the investigation of transport properties such as the thermal diffusivity of optically transparent fluids. The main advantages of the method are its quickness, the fact of the thermodynamic state of equilibrium of the sample (gradients are not required), and the relatively simple evaluation of data without the necessity of calibration. However, an insufficient production of intensity of scattered light may be a limiting effect. For that reason the vicinity of the gas–liquid critical point represents the classical range of application. In this paper, it is shown that by means of an appropriate choice of experimental apparatus, measurements are also feasible in an extended range of states. Broad regions around critical points of three pure fluids (sulfur hexafluoride, SF_6; ethane, C_2H_6; nitrous oxide, N_2O) over temperature ranges $|T - T_c|$ of 0.02 to 50 K and density ranges (ρ/ρ_c) of 0.2 to 2 were investigated. In this region the thermal diffusivity shows great variations with temperature and density and cannot be described by means of ideal-gas behavior or relations for liquids. The measurements were carried out along the coexistence curve for both phases, along the critical isochore and along some isotherms with $T \lesssim T_c$. The measured or calculated density, pressure, and thermal diffusivity data as well as some correlations are presented.

KEY WORDS: dynamic light scattering; ethane; gas–liquid critical point; nitrous oxide; sulfur hexafluoride; thermal diffusivity.

1. INTRODUCTION

The best possible knowledge of the thermophysical properties of working substances is necessary for the optimum operation of any component in power industries. Usually, it is possible to obtain thermodynamic properties of different fluids, but often transport properties are not available. In

[1] Lehrstuhl A für Thermodynamik, Technische Universität München, Arcisstr. 21, D-8000 München 2, Federal Republic of Germany.

0195-928X/87/0200-0165$05.00/0

such cases, one can make use of the known relations for liquids or perfect gases to estimate the property. However, these relations will break down near the critical point. As shown in Fig. 1, the thermal diffusivity, a, of water, for instance, exhibits a strong singularity near this point [1]. On the other side a universal critical behavior in a large variety of physical systems is expected. This distinguishes the critical point and is certainly one reason for the frequent use of it as a central point in different types of equations of state.

In this paper, our thermal diffusivity measurements very close to the critical point as well as in an extended region are presented. The covered temperature ranges were $0.02 \lesssim |T - T_c| \lesssim 50$ K; the density ranges, $0.2 \lesssim \rho/\rho_c \lesssim 2$. Each of the three pure fluids sulfur hexafluoride (SF_6), ethane (C_2H_6), and nitrous oxide (N_2O) was investigated along both phases of the coexistence curve, along the critical isochore, and along some isotherms with $T \lesssim T_c$ (subscript c represents critical values).

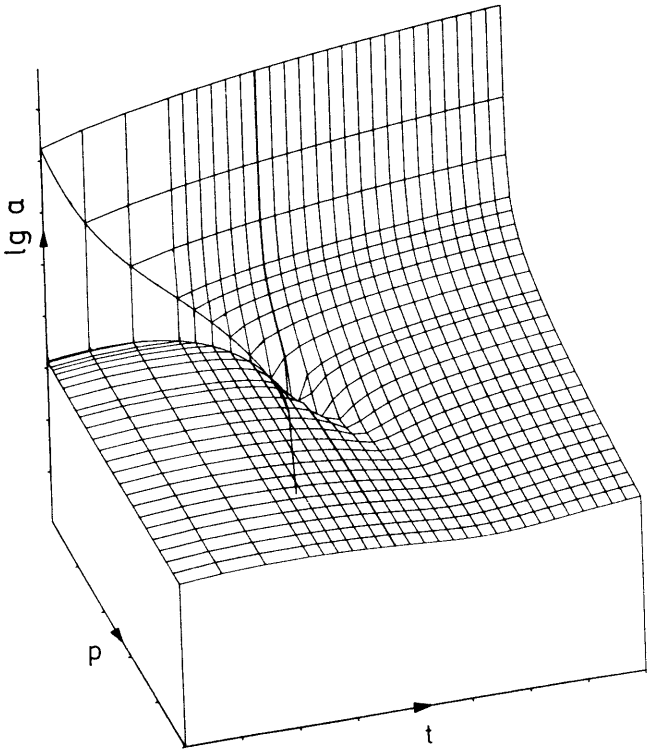

Fig. 1. Thermal diffusivity of water temperature and pressure [1].

The temperature, pressure, and refractive index were measured, and from them the density and the isothermal compressibility were calculated. Measurements of the thermal diffusivity were carried out by means of a dynamic light-scattering apparatus. Some correlations for those results are given.

The crucial point of the paper is not to describe experimental details but to present thermodynamically consistent sets of data with different properties of three fluids.

2. THEORY OF DYNAMIC LIGHT SCATTERING

An exact description of the theory of light scattering is given by Berne and Pecora [2], Cummins and Pike [3], and Chu [4], for example. In this paper, only some topics should be explained which seem to be necessary for an appreciation of following sections.

Because of the permanently existing random motion of all molecules, even in a macroscopic state of equilibrium, an optical inhomogenety of the fluid is produced which scatters incident light in all directions. The electric field of the scattered light at a large distance R from the scattering volume is

$$\vec{E}_s(\vec{R}, t) = \frac{\vec{E}_0}{4\pi\varepsilon_0} \exp(i\vec{k}_s \vec{R}) \int \exp[i(\vec{q}\vec{r} - \omega t)]\, \Delta\varepsilon(\vec{r}, t)\, d^3r \tag{1}$$

where t is the time, $\vec{E}_0$ is the amplitude vector of the incident electric field, $\vec{k}_s$ is the wave vector of the scattered light, and ω is the light frequency. The scattering vector $\vec{q}$ is determined by

$$|\vec{q}| = \frac{4\pi n}{\lambda_L} \sin\left(\frac{\theta}{2}\right) \tag{2}$$

where n, λ_L, and θ are the refractive index of the fluid, the wavelength of the light, and the scattering angle, respectively. $\vec{E}_s(\vec{R}, t)$ depends on $\Delta\varepsilon(\vec{r}, t)$, the fluctuation in the dielectric constant $\varepsilon(\vec{r}, t) = \varepsilon_0 + \Delta\varepsilon(\vec{r}, t)$, which brings about the optical inhomogenety. ε_0 is the constant-equilibrium value.

In light-scattering experiments only the spatial Fourier component of the total spectrum due to the scattering angle θ is detected. Introducing the Fourier transformation

$$\Delta\tilde{\varepsilon}(\vec{q}, t) = \int \exp(i\vec{q}\vec{r})\, \Delta\varepsilon(\vec{r}, t)\, d^3r \tag{3}$$

and the scattered intensity $I_s(\vec{R}, t) \sim |\vec{E}_s(\vec{R}, t)|^2$ to Eq. (1) yields

$$I_s(\vec{R}, t) \sim |\Delta\tilde{\varepsilon}(\vec{q}, t)|^2 \tag{4}$$

The temporal behavior of the intensity of scattered light is determined by the temporal behavior of the fluctuations in ε.

The reasons for dielectric fluctuations are fluctuations in the properties of state, which statistically regress back to equilibrium due to the same equations which describe macroscopic relaxation processes [5]. The consequence is an exponential decay of $\Delta\tilde{\varepsilon}(\vec{q}, t)$ with a relaxation time aq^2 in single-component fluids, where a is the thermal diffusivity.

Because of the stochastic process it is not possible to observe a single dielectric fluctuation. Hence the autocorrelation function is calculated from the scattered intensity

$$c(t^*) = \lim_{t' \to \infty} \frac{1}{t'} \int_0^{t'} I_s(t)\, I_s(t + t^*)\, dt \tag{5}$$

It contains information about the influence of the value I_s at any moment on the same value t^* afterward. According to Eq. (4) and above explanations, $c(t^*)$ decays like an exponential function with a relaxation time of $\frac{1}{2}aq^2$. The fitting procedure yields a and information about deviations from the ideal form. They are due to effects such as stray light from the windows (heterodyning). The criterion for the statistical reliability is the calculated correlation coefficient. Only results with coefficients greater than 0.99 are used.

3. EXPERIMENTAL APPARATUS

Figure 2 shows the dynamic light-scattering apparatus schematically (see also Ref. 6). A homodyne method is used with a digital correlator for the calculation of the time autocorrelation function according to Eq. (5). The scattering angle θ is adjustable optionally (normally $\pm 8...10°$) by means of a revolving table and determined within an angle range of 6 s. The classical range of application of dynamic light scattering is the vicinity of critical points because of high scattered intensity. The extended range of application of our apparatus is provided by a high laser power (with quick measurements because of heating effects), a highly sensitive detector with a low noise level, small scattering angles, and therefore a sufficient length of the sample cell and, additionally, by using a pinhole (6), which is advantageous for screening stray light from the sample-cell windows.

The refractive index of the fluid is needed for the calculation of the scattering vector and the density. Measurements are done by a simple refractometer shown in Fig. 3. The registered wavelength of the Hg-spectral lamp is $\lambda = 546.1$ nm.

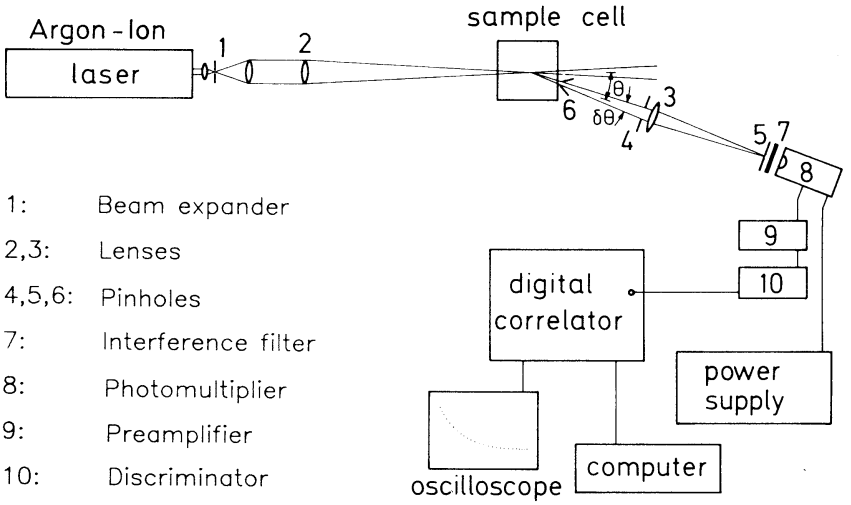

Fig. 2. Schematic diagram of dynamic light-scattering apparatus.

The sample cell is designed for a maximum pressure of 120 bar. Temperature and pressure are measured by thermocouples (accuracy, about ± 0.02 K) and pressure transducers (accuracy, about ± 0.1 bar), respectively.

4. EXPERIMENTAL RESULTS

Three pure fluids were investigated: sulfur hexafluoride (SF_6), ethane (C_2H_6), and nitrous oxide (N_2O).

All measurements were carried out along both phases of the coexistence curve, the critical isochore, two isotherms with $T > T_c$, and two isotherms with $T < T_c$.

The values of critical temperatures t_c, critical pressures p_c, critical densities ρ_c, and critical refractive indices n_c are shown in Table I.

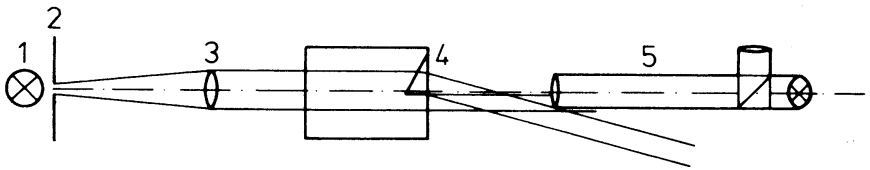

Fig. 3. Schematic diagram of refractometer: 1, Hg-spectral lamp; 2, slit; 3, lens; 4, prism; 5, autocollimating telescope.

Table I. Parameters for SF_6, C_2H_6, and N_2O

	SF_6	C_2H_6	N_2O	Notes
t_c (°C)	45.52	32.15	36.45	
p_c (bar)	37.64	48.26	71.67	Ref.
ρ_c (kg · m^{-3})	741.	206.	457.	Ref. 14
n_c	1.0891	1.1208	1.1186	
M (kg · kmol^{-1})	146.	30.07	44.02	Ref. 14
LL (10^{-3} m^3 · kmol^{-1})	11.51	11.48	7.44	Eq. (6)
A	0.722	0.701	0.730	Eq. (7)
B	3.74	3.73	3.78	Eq. (9)
β	0.338	0.350	0.349	Eq. (9)
a_0 (10^{-6} m^2 · s^{-1})	0.704	1.10	0.635	Vapor,
φ	0.883	0.893	0.849	Eq. (11)
a_0 (10^{-6} m^2 · s^{-1})	0.201	0.288	0.165	Critical isochore,
φ	0.831	0.819	0.776	Eq. (11)
a_0 (10^{-6} m^2 · s^{-1})	0.723	1.04	0.424	Liquid,
φ_0	0.890	0.886	0.800	Eq. (11),
φ_1	3.96	3.25	0.703	Eq. (12)

4.1. Density

The density ρ is calculated from the measured refractive index n. Both are connected by the Lorentz–Lorentz relation

$$\rho = \frac{n^2 - 1}{n^2 + 2} \frac{M}{\mathrm{LL}} \tag{6}$$

where M is the molecular mass and LL is the Lorentz–Lorenz function. According to Rathjen and Straub [7], LL should be constant for the liquid as well as for the gaseous phase even close to the critical point. The applied values of LL and M are shown in Table I.

Along the critical isochore the refractive index is $n = n_c$ = constant. The results of measurements along isotherms are presented in Section 4.2. Figure 4 shows calculated densities for both phases of the coexistence curve versus temperature for all three substances. The densities are divided by the critical densities (see Table I). The straight lines in Fig. 4 represent the average of vapor densities ρ'' and liquid densities ρ' and are described by the rule of Cailletet-Mathias:

$$\frac{\rho' + \rho''}{2\rho_c} = 1 + A\,|\tau| \tag{7}$$

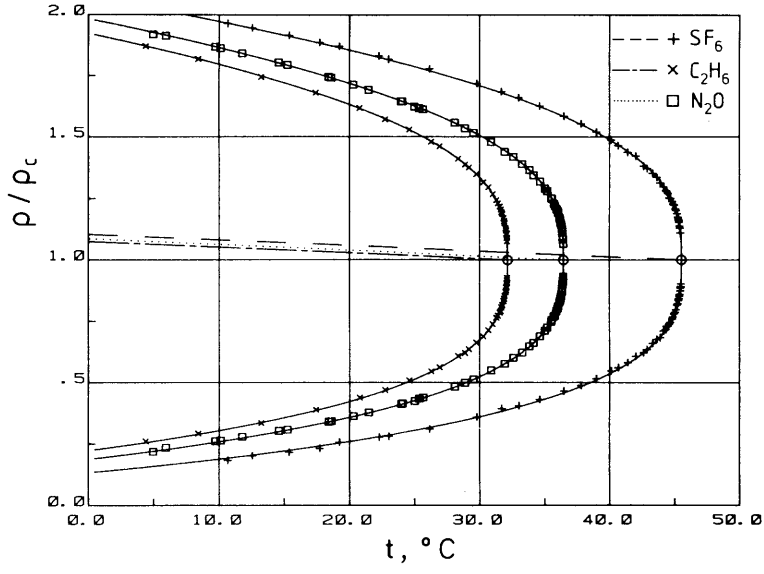

Fig. 4. Reduced density versus temperature for coexisting liquid and vapor for SF_6, C_2H_6, and N_2O.

where τ is the reduced temperature difference,

$$\tau = \frac{T - T_c}{T_c} \tag{8}$$

A is a constant which is listed in Table I.

The difference between liquid and vapor densities should satisfy the critical power law

$$\frac{\rho' - \rho''}{\rho_c} = B\,|\tau|^{\beta} \tag{9}$$

The fitted data lead to parameters B and β as shown in Table I. Figure 5 presents these data double logarithmically in comparision with Eq. (9) for all three substances versus $|\tau|$. The agreement is very good. According to the universality hypothesis [8], the critical exponent β should be the same for all fluids. It can be predicted theoretically by different means such as the solution of the three-dimensional Ising model or renormalization methods. The estimated value is about 0.325. The averaged value of β from our measurements of SF_6, C_2H_6, and N_2O is 0.345 ± 0.005. It runs a little higher than the theoretically predicted value but agrees well with most of other experimental results (e.g., Refs. 7, 9, and 10).

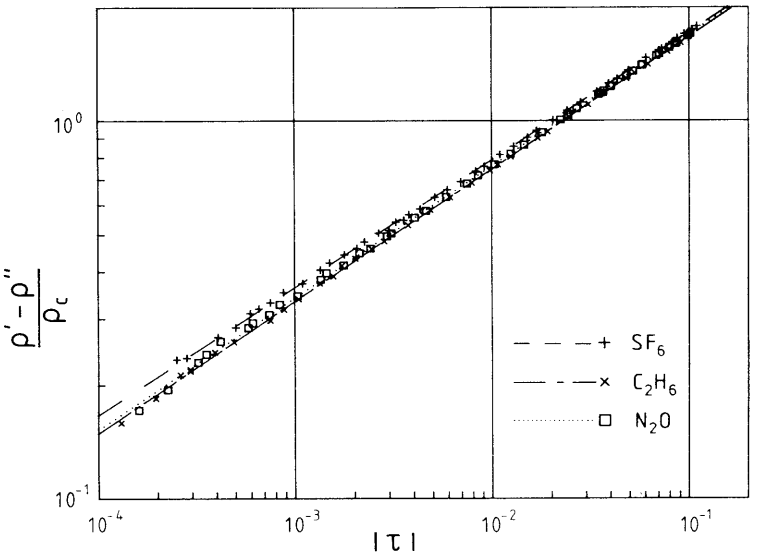

Fig. 5. Reduced density difference between coexisting liquid and vapor versus reduced temperature difference for SF_6, C_2H_6, and N_2O.

4.2. Pressure

Pressure–density diagrams are suitable for an illustration of the investigated range of state. Every symbol implies one performed measurement of the thermal diffusivity. Figure 6 presents the reduced pressure p/p_c versus the reduced density ρ/ρ_c for sulfur hexafluoride. All investigated paths, the coexistence curve, the critical isochore, and the four isotherms, are shown. The isotherms are chosen to have reduced temperature differences τ according to Eq. (8) of $\pm 10^{-2}$ and $\pm 10^{-3}$. For comparison, values of pressure calculated from a Benedict–Webb–Rubin equation of state [11] are shown. The agreement is very good.

From measured p, ρ data the isothermal compressibility along all isotherms can be calculated. This function is very important for light-scattering experiments since the scattered intensity is proportional to it. Sufficient intensities are necessary for the practicability of the described method to measure thermal diffusivities. In our experiments we covered a range of compressibilities of about three orders of magnitude. The results as well as p, ρ data of C_2H_6 and N_2O are not presented here because this would exceed the limited scope of this paper.

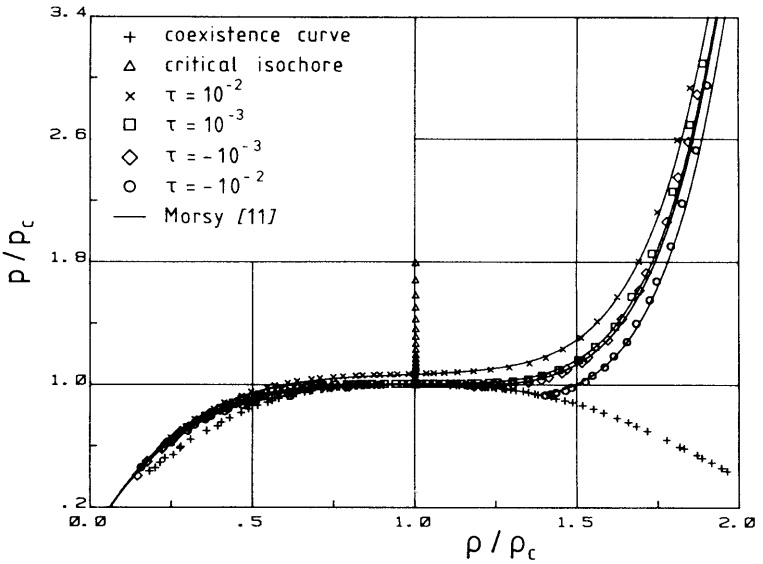

Fig. 6. Reduced pressure versus reduced density for SF_6.

4.3. Thermal Diffusivity

As described above, difficulties in the application of dynamic light scattering arise from small scattered intensities. Decreasing isothermal compressibilities and therefore decreasing scattered intensities are caused by increasing density differences $\rho - \rho_c$. In Section 3, all precautions taken were shown to extend the classical range of application of the method, which is represented by the vicinity of the critical point. As may be seen from Fig. 6, a density range $0.2 \lesssim \rho/\rho_c \lesssim 2$ is covered, and temperature differences vary between $0.02\ \mathrm{K} \lesssim |T - T_c| \lesssim 50\ \mathrm{K}$ (the lower limit of 0.02 K is due to the above-mentioned accuracy in temperature measurements). Because of the great variations of thermal diffusivity, a, in this region, a logarithmic presentation seems to be significant. Figure 7 shows measured thermal diffusivities, a, of the coexistence curve and the isotherms of each of the three substances versus reduced density ρ/ρ_c. Critical isochore data are shown in the next section.

In Fig. 7 no comparison with literature data is given because this was performed in a previous publication [12] with the aid of SF_6. Additionally, prior measurements on the ethane critical isochore should be mentioned [15, 16], which agree well with the presented data.

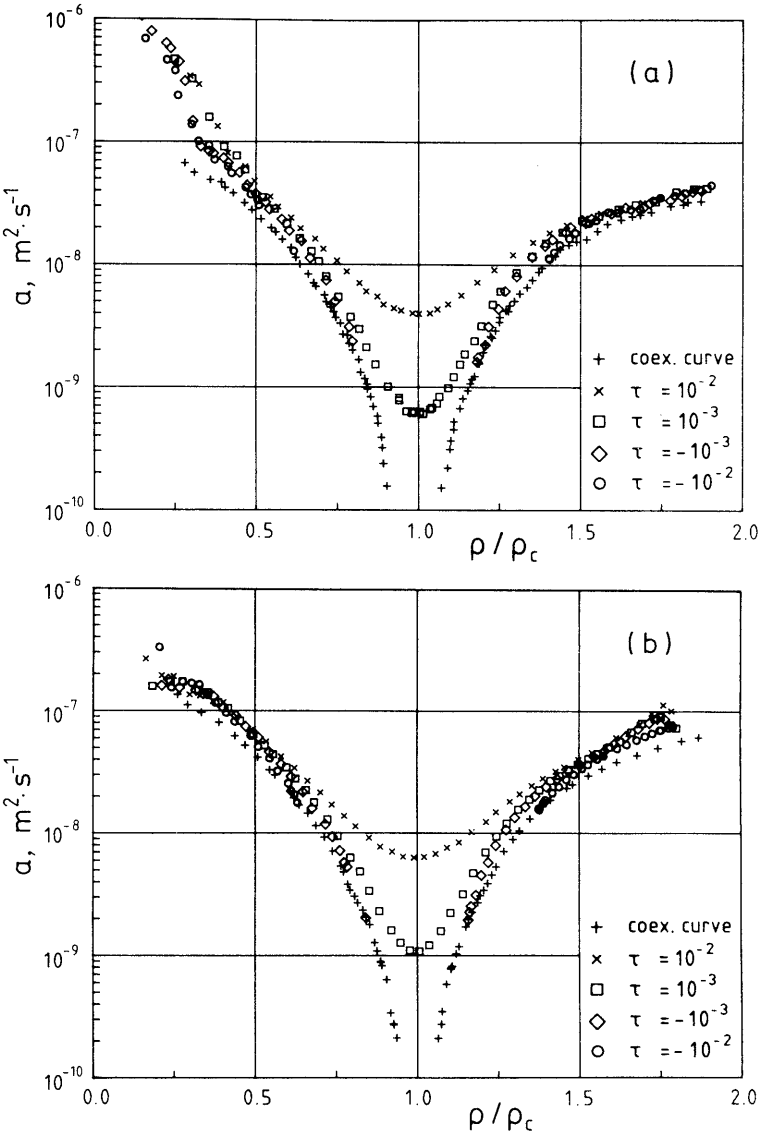

Fig. 7. Thermal diffusivity versus reduced density for SF_6 (a), C_2H_6 (b), and N_2O (c).

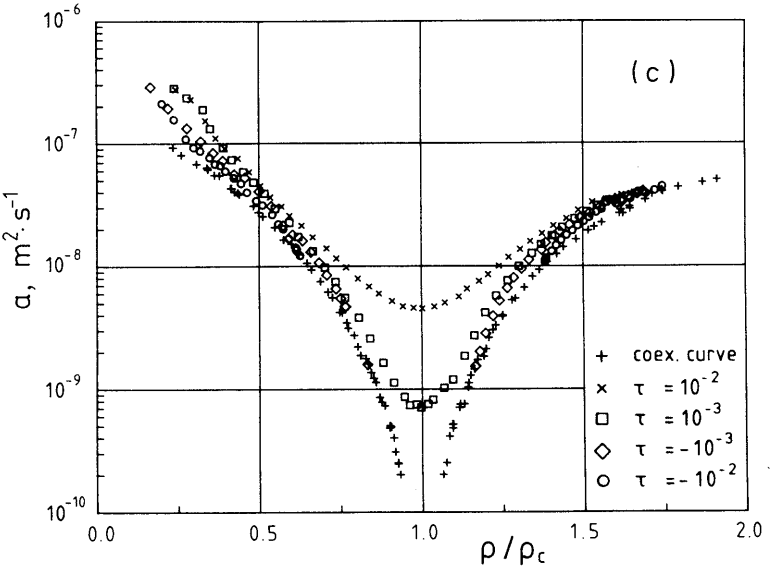

Fig. 7 (*continued*)

5. DISCUSSION OF THERMAL DIFFUSIVITY DATA

The thermal diffusivity, a, is related to the thermal conductivity coefficent λ and the specific heat at constant pressure c_p

$$a = \frac{\lambda}{\rho c_p} \tag{10}$$

In the vicinity of the critical point it decreases rapidly. Its temperature behavior can be described analogous to Eq. (9) by a power-law relation

$$a = a_0 |\tau|^{\varphi} \tag{11}$$

for both phases of the coexistence curve and for the critical isochore. Figure 8 presents the thermal diffusivity, a, double logarithmically versus the reduced temperature difference for each of the three fluids except for the isotherms. Some consequences are evident.

(a) With the approach of the critical point the thermal diffusivities of liquid and vapor are very similar for about $|\tau| \lesssim 10^{-2}$.

(b) All measured data for the critical isochore and the gaseous phase are represented very well by Eq. (11). Both paths lead to similar exponents φ.

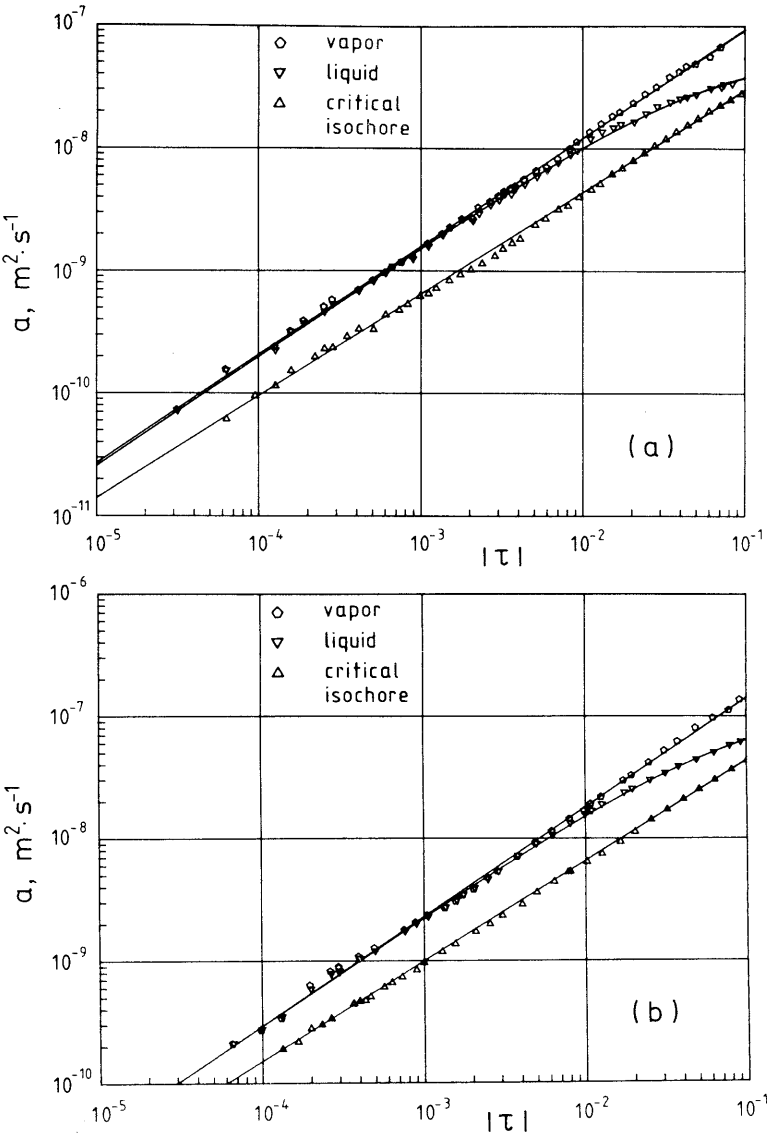

Fig. 8. Thermal diffusivity versus reduced temperature difference for SF_6 (a), C_2H_6 (b), and N_2O (c).

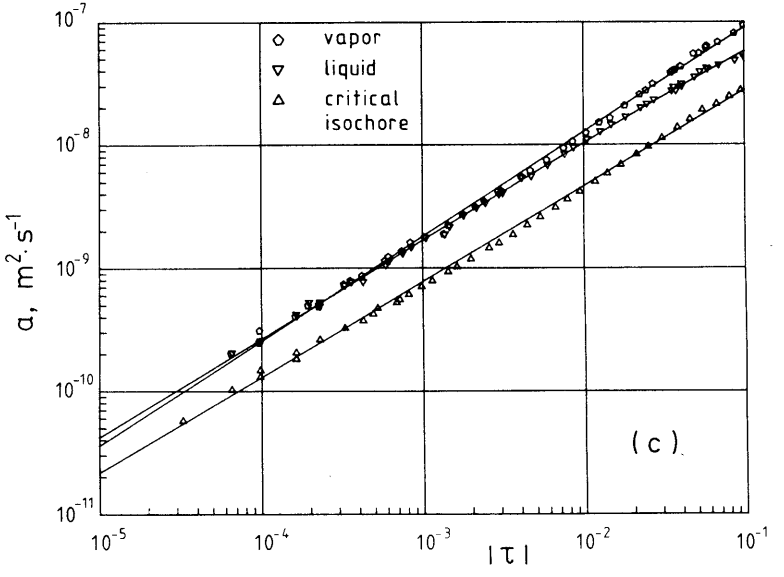

Fig. 8 (*continued*)

(c) Above $|\tau| \approx 10^{-2}$, thermal diffusivities of the liquid phase deviate clearly from the straight line according to Eq. (11). This can be described by a simple modification of the exponent,

$$\varphi = \varphi_0 + \varphi_1 |\tau| \qquad \text{(liquid)} \tag{12}$$

(d) Each of the three fluids shows the same temperature dependence of thermal diffusivity, a; the exponents are almost identical. Differences in virtue of molecular properties appear only in the amplitude a_0.

All measured data were fitted with Eqs. (11) and (12) for lowest standard deviations. The obtained coefficients are shown in Table I. The average of all calculated φ and φ_0 is 0.85 ± 0.02. This value runs a little higher than the theoretically predicted value of about 0.67 [13], which is calculated from power-law relations for λ and c_p. These relations refer only to the anomalous contributions to the thermal conductivity λ and the specific heat c_p. In doing so the error produced is very small for c_p because it diverges strongly with insignificant background effects. In opposition to this, the divergence of λ is weak, and the background effect is important. Therefore the critical (negative!) exponent for λ is greater than that of the anomalous contribution, and the resulting exponent of the thermal dif-

fusivity according to Eq. (10) must be higher than the theoretically predicted one. It should be mentioned that the presented treatment of data does not agree with above-described practices in critical phenomena on purpose. In this paper we want just to give empirical correlations to describe the thermal diffusivity behavior in a wide range of states. A critical-exponent analysis with the use of modern techniques will be realized in a later paper.

From the a versus ρ/ρ_c plots (Fig. 7) also, some conclusions can be drawn.

(a) For a constant density all thermal diffusivity data, not only for isotherms above T_c but also for isotherms below T_c, are greater than that of the saturated liquid or vapor.

(b) Values of a along isotherms with $T < T_c$ approach those of the coexistence curve and coincide at phase equilibrium.

(c) Values of a along isotherms with $T > T_c$ show an increasing decay with decreasing temperature differences $T - T_c$ for densities close to ρ_c.

(d) The behavior of all isotherms is much similar for great density differences $|\rho - \rho_c|$.

(e) Each of the three fluids shows the same density dependence of a; only the absolute values differ.

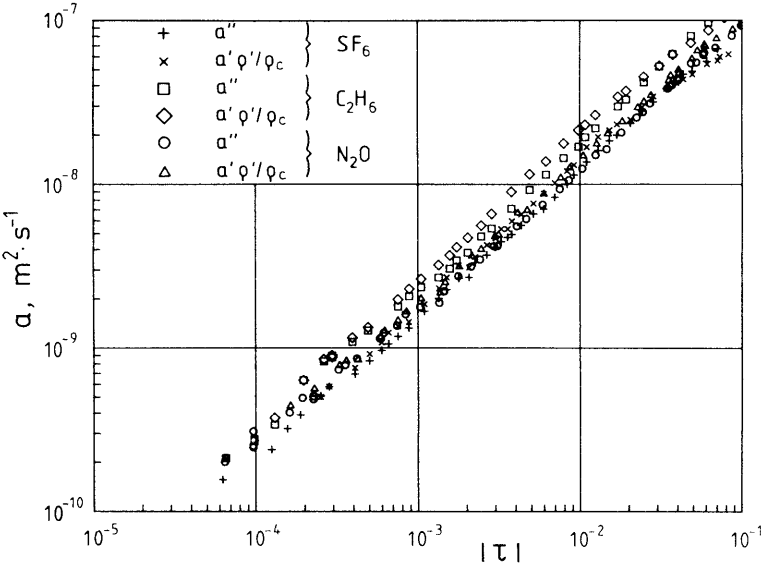

Fig. 9. Thermal diffusivity versus reduced temperature difference for SF_6, C_2H_6, and N_2O.

Some speculative considerations should be made here. Our actual objective of interest is an equation which describes the thermal diffusivity as a function of density and temperature. It should cover the investigated range of states and should link it with liquid and gas behavior far from the critical point. It is obvious from Figs. 7 and 8 that in those regions the thermal diffusivity of the liquid tends toward a constant level, while the thermal diffusivity of the gas increases continuously. This is also evident from Fig. 1. The assumption that this increase is derived mainly from the density decrease is confirmed by Figs. 9 and 10. Figure 9 presents the thermal diffusivity of both coexisting phases for all three substances double logarithmically versus the reduced temperature difference. In opposition to Fig. 8, the thermal diffusivity value for the liquid a' is multiplied by the reduced liquid density ρ'/ρ_c. The temperature behavior of the liquid is now very similar to that of the vapor. From Fig. 10 the same conclusion can be drawn. It presents the thermal diffusivity logarithmically versus the reduced density difference $|\rho/\rho_c - 1|$. Once more, all values for the liquid a' are multiplied by ρ'/ρ_c. The density dependence of a for both phases is now almost the same; a'' for the vapor and $a\,\rho'/\rho_c$ for the liquid are symmetrical to the $\rho/\rho_c = 1$ axis.

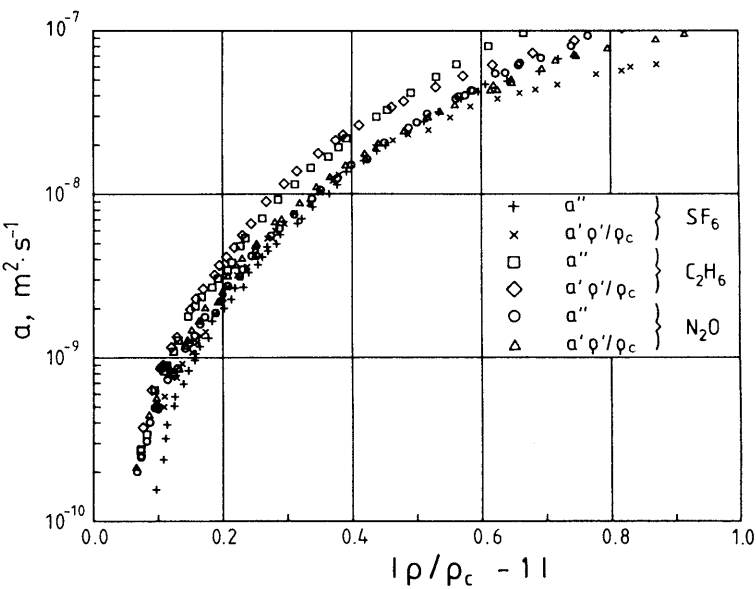

Fig. 10. Thermal diffusivity versus reduced density difference for SF_6, C_2H_6, and N_2O.

Analogous conclusions can be drawn from the investigated isotherms but the presentation in this paper would lead too far. We hope that we will soon be able to specify correlations for a which cover the whole investigated range of states.

6. CONCLUSIONS

(a) The average density of both coexisting phases is well described by the Cailletet–Mathias relation [Eq. (7)].

(b) The temperature behavior of the reduced density difference of both coexisting phases is universal and is covered by a power-law relation, Eq. (9). The average critical exponent is 0.345 ± 0.005.

(c) In the investigated range of state the $p(\rho)$ dependence for SF_6 is compared with Morsy's equation of state; the agreement is very good.

(d) The behavior of the thermal diffusivity in the vicinity of the critical point and its link to the ranges of gas and liquid were discussed in detail (Section 5). All three substances show very similar dependences; they differ only in their absolute values.

(e) Correlations $a(\tau)$ are given for both coexisting phases and the critical isochore.

REFERENCES

1. P. Schiebener, *Proc. 10th Int. Conf. Prop. Steam* (Moscow, 1984, in press); Private communication, Technical University Munich (1984).
2. B. J. Berne and R. Pecora, *Dynamic Light Scattering* (Wiley, New York, 1976).
3. H. Z. Cummins and E. R. Pike; *Photon Correlation and Light Beating Spectroscopy* (Plenum Press, New York, 1974).
4. B. Chu, *Laser Light Scattering* (Academic Press, New York, 1974).
5. L. Onsager, *Phys. Rev.* **37**:405 (1931); **38**:2265 (1931).
6. E. Reile, *Messung der Temperaturleitfähigkeit reiner Fluide und binärer Gemische mit Hilfe der dynamischen Lichtstreuung in der weiteren Umgebung des kritischen Punktes*, Thesis (Technical University Munich, Munich, 1981); E. Reile, P. Jany, and Straub, and J. Straub, *Wärme. Stoffübertr.* **18**:99 (1984).
7. W. Rathjen and J. Straub, *Proc. 7th Symp. Thermophysical Prop.*, A. Cezairliyan, ed. (ASME, New York, 1977), p. 839; *Wärme. Stoffübertr.* **14**:59 (1980).
8. J. V. Sengers, *Proc. Cargese Summer Inst. Phase Trans.*, M. Levy, J. C. Le Guillou, and J. Zinn-Justin, eds. (Plenum, New York, 1980).
9. J. C. Guillou and J. Zinn-Justin, *Phys. Rev. B* **21**:3976 (1980).
10. J. K. Tison and E. R. Hunt, *J. Chem. Phys.* **54**:1526 (1971).
11. T. E. Morsy, *J. Chem. Eng. Data* **15**:256 (1970).
12. P. Jany and J. Straub; *Proc. 10th Int. Conf. Prop.* of *Steam* (Moscow, 1984, in press).
13. J. V. Sengers and P. H. Keyes, *Phys. Rev. Lett.* **26**:70 (1970).
14. Landolt-Börnstein, *Zahlenwerte und Funktionen* (Springer, Berlin, 1969).
15. R. F. Chang and T. Doiron, *Proc. 8th Symp. Thermophysical Prop.*, J. V. Sengers, ed. (ASME, New York, 1982), p. 458.
16. R. Tufeu and B. Le Neindre, *High Temp.-High Press.* **13**:31 (1981).

Printed by the St. Catherine Press Ltd., Tempelhof 41, Bruges, Belgium